Chemical Physics 158 (1991) 249–260
North-Holland

Protein relaxation dynamics in human myoglobin

David G. Lambright, Sriram Balasubramanian and Steven G. Boxer [1]
Department of Chemistry, Stanford University, Stanford, CA 94305, USA

Received 24 June 1991

Transient absorption spectra in the Soret region have been measured following the photolysis of human MbCO in 75%(w/w) glycerol:water at 250, 270, and 290 K. The peak of the transient difference spectrum near 436 nm shifts from low to high energy on the nanosecond time scale. The spectral changes are quantitatively analyzed using an approach based on singular value decomposition, and the results are interpreted in terms of a structural relaxation of the protein. The kinetics of the relaxation and ligand rebinding are nonexponential in time. At all three temperatures, the relaxation is complete prior to the end of the geminate phase of recombination. At 250 K the transient spectra have relaxed to the equilibrium deoxyMb–MbCO spectrum after 10 μs. At 290 K the relaxation is faster and is complete on the ns time scale. The kinetics of the geminate recombination following the spectral changes are single exponential.

1. Introduction

The binding of diatomic ligands to heme proteins is accompanied by rearrangements in tertiary [1–5] and, in the case of hemoglobin (Hb), quaternary structure [6,7]. Of particular interest is the role of protein dynamics in these reactions. One of the simplest and best characterized protein–ligand reactions is the recombination of CO to myoglobin (Mb) following photolysis of the iron–CO bond. The role for protein dynamics arises naturally in at least two aspects of the recombination reaction: in the diffusion of the ligand between the heme pocket and solvent [3,8] and in the relaxation of the protein structure on going from the ligated to the unligated form.

Since the seminal experiments of Gibson [9], the recombination of CO to Mb following photolysis of the Fe–CO bond has been extensively investigated by a variety of spectroscopic techniques over a wide range of timescales, temperatures, and solvent conditions [10–13]. In glycerol:water glasses at temperatures below 200 K, the kinetics of the recombination process are highly nonexponential and independent of ligand concentration [10]. A charge transfer band near 760 nm in deoxyMb (but not present in MbCO) has been shown to be shifted to low energy in the photoproduct spectrum compared with the equilibrium spectrum at 4 K [14]. Values reported for this shift range from 116 cm^{-1} [15] to over 200 cm^{-1} [14]. At temperatures up to 200 K, this band exhibits a time-dependent shift from low to high energy following photolysis [16]. This was initially interpreted as a structural relaxation based on the difference between the photoproduct spectrum and the deoxyMb spectrum [14] and on the time-dependent shift [16]. Subsequent experimental [17] and theoretical [18] work showed that the changes in the first and second moments of the band were consistent with a reactive line-narrowing interpretation (also called kinetic hole burning). These experiments suggest a correlation between electronic transition energies and the rate of rebinding such that molecules with lower transition energies react faster giving rise to a shift and narrowing of the band. A time dependent shift in the Soret region at 40 K has also been reported, but the correlation between the shift and kinetics was said to be weak [19]. Evidence for relaxation in the liganded state has been reported [20]. Multiple relaxation processes in the response of MbCO to a sudden change in pressure have been observed near the glass transition temperature of glycerol:water [21]. These relaxation processes in-

#1 To whom correspondence should be addressed.

clude the interconversion amongst the various CO conformers [20,21].

These observations contrast with the much simpler behavior in aqueous solution at room temperature. Ultrafast transient absorption measurements have shown that a photoproduct with a deoxy-like absorption spectrum appears within 350 fs [22]. Vibrational cooling of the photoproduct occurs in less than 10 ps [23], and a transient spectrum similar to the equilibrium deoxyMb–MbCO spectrum is observed at 30 ps [24]. Although other diatomic ligands such as O_2 and NO exhibit picosecond recombination processes, no recombination has yet been observed for CO on this time scale. In a careful study of the transient absorption spectra at room temperature on the ns to ms time scale, Henry et al. [25] observed a 4% geminate process for CO with a time constant of 180 ns. Most of the dissociated CO molecules escape into bulk solvent, and a subsequent recombination process (dependent on the concentration of CO) is observed.

Transient absorption and resonance Raman spectra of photolyzed MbCO in aqueous solution at room temperature are very similar to the equilibrium spectra by 30 ps [24–27]. A few reports, however, have indicated the possibility of unrelaxed intermediates on the ns [25,28] and ps timescales [29]. A 700 ns process has been observed in photoacoustic experiments [30], and recently evidence for structural relaxation of the globin on the ps time scale has been obtained from transient grating [31] and transient CD experiments [32]. Local structural changes on the ps time scale involving the iron-proximal histidine coordinate have also been suggested based on molecular dynamics simulations and the nonexponential rebinding of NO [33].

In addition to the experimental data, several theoretical models have been put forward to explain the rebinding of CO to Mb. In the two-dimensional model of Agmon and Hopfield [34] all conformational degrees of freedom are lumped together in a single coordinate. Srajer et al. have proposed a more specific model which treats the iron out of plane displacement as an important and independent degree of freedom [35]. Recently, Steinbach et al. [15] have developed an empirical model based on a large number of experimental observations including distributed rebinding, kinetic hole burning, the spectral evolution of the 760 nm band, and the anomalous temperature dependence of the rebinding kinetics in the region of the glass transition temperature. Although parameters from these models have been extrapolated to room temperature, detailed experimental data in the temperature range between 220 K and room temperature have been limited primarily to the measurement of single wavelength kinetics [10,15]. Consequently, little direct experimental information on the relaxation processes is available in this temperature range.

The present study examines the transient absorption spectra of photolyzed MbCO on the ns to ms time scale in a 75%(w/w) glycerol:buffer solvent system between 250 and 290 K. The transient spectrum at 10 ns is not fully relaxed and analysis of the data by singular value decomposition reveals that the temporal evolution of the metastable photoproduct spectrum is characterized by a single spectral change. The results are interpreted in terms of a structural relaxation which is connected with the process of ligand recombination. A comparison is made with the relaxations observed in sperm whale Mb and MbCO below 220 K [15,20,21] and with the deoxy Hb spectral changes observed in aqueous solution at room temperature [36–38]. These results set the stage for related experiments on a variety of human Mb mutants to be presented elsewhere [39].

2. Experimental

2.1. Sample preparation

Details of the expression and purification of human Mb were described earlier [40,41]. The recombinant human Mb protein used in these experiments is a site specific mutant of the wild-type protein in which the cysteine at position 110 has been replaced with alanine in order to eliminate the problem of cysteine oxidation during purification. Alanine is the naturally occurring residue at this position in nearly all other Mbs including sperm whale Mb. The properties of this mutant are very similar to those of the native protein and, hereafter, it will be referred to simply as Mb. A concentrated stock solution of the protein was prepared by anion exchange chromatography on a DE-52 column (Whatman) which had

been equilibrated with 5 mM Tris buffer at pH 9.0. The protein was eluted as a single band with 100 mM potassium phosphate buffer at pH 7.0. A small aliquot of the concentrated metaquo Mb solution was diluted into a deoxygenated solvent system of 75%(w/w) glycerol/water buffered with 100 mM potassium phosphate, pH 7.0. The glycerol solvent was deoxygenated by stirring under argon for 1 day. For MbCO samples, the glycerol solution was stirred for an additional day under 1 atm of CO. The protein was reduced by addition of sodium dithionite to a final concentration of 10 mM.

2.2. Transient absorption measurements

Samples of MbCO in 1 mm path length quartz cells were excited at 532 nm with 8 ns fwhm pulses from a Q-switched Nd:YAG laser (Quantel). The energy density of the pulses was 40 mJ/cm^2 at the sample. Broadband cw light from a 500 W xenon arc lamp was focused onto the entrance slit of a 0.22 m single monochromator (500 nm ruled grating). Light from the exit slit of the monochromator was collimated and focused to an image at the sample. The power density of the probe light was 200 μW/cm^2 and had a spectral bandwidth of 4.5 nm. The detector was protected from scattered excitation light by two 80 nm fwhm interference filters with maximum throughput at 400 nm. Signals were detected in transmission using an FND-100 silicon photodiode (EG&G) reverse biased at 45 V. A CLC-205 hybrid op-amp (Comlinear) in the inverting configuration was used to convert the small photodiode current to a voltage with a transresistance of 2.5 kΩ. A second CLC-205 was used in the non-inverting configuration to provide a 20-fold amplification. In order to optimize performance, the components were assembled on a custom designed PC board inside an aluminum chassis which served as an rf shield. An L–C filter on the power supply lines to the detector eliminated rf pickup from the flash lamps of the laser. Transient signals were digitized on a dual time base using a Tektronix DSA602 oscilloscope. Acquisitions were triggered by reflecting a small portion of the exciting pulse onto a second photodiode. The trigger jitter was <1 ns. Signals were averaged 128 to 1000 times at a repetition rate of 2–10 Hz. The impulse response of the detector measured with an 80 ps laser diode has a fwhm of 4 ns. The instrument response (including timing jitter), measured by scattering a small amount of light from the YAG laser excitation source onto the detector, has a nearly Gaussian profile with a fwhm of 9 ns. The step response of the instrument was measured using a sample of heme–CO in 100 mM Tris buffer at pH 9.0. The step response consists of an overshoot of 1–2% which settles to within 1% of its final value in 22 ns and within 0.2% (the limit of detection) within 50 ns.

2.3. Acquisition of transient spectra

Transient spectra were reconstructed from single wavelength measurements taken at 1 nm intervals in a pseudo-random order. Typical data sets consisted of transient absorption measurements at 61 wavelengths between 399 and 459 nm requiring approximately 2 h to acquire at a repetition rate of 10 Hz. The data collection process was fully automated by using an IBM PC as the controller to drive the monochromator and to optimize the vertical settings for the oscilloscope at each new wavelength. Transmitted intensities $I(\lambda, t)$ were converted to ΔA according to:

$$\Delta A(\lambda, t) = -\log_{10}[I(\lambda, t)/I_{bas}(\lambda)] , \qquad (1)$$

where $I_{bas}(\lambda)$ is the transmitted intensity prior to the excitation pulse. Zero time was chosen to correspond to the midpoint of the rising edge of the trace with the highest S/N ratio. In order to obtain computationally manageable data sets, the number of points in the time domain was reduced from 4096 (2048 on each time base) to 256 by selecting points on a log scale. This was done without averaging adjacent points to avoid possible smoothing artifacts.

2.4. Correction for spectral bandwidth

A small distortion in the shape of the spectra is present as a result of intensity averaging over the finite spectral bandwidth. Because the effect is small ($<3\%$ at any wavelength), a zeroth-order approximation for the distortion can be obtained from the difference between the measured intensities and the convolution of the measured intensities with the slit function of the monochromator. When the measured intensities are corrected using this zeroth-order ap-

proximation to the distortion, the rank of the data matrix as assayed by singular value decomposition (see below) is reduced from three to two accompanied by the disappearance of a slight wavelength dependence previously observed in the kinetics of the bimolecular process.

2.5. Correction for photoselection

In order to account for the photoselection introduced by the linearly polarized excitation pulses [42,43], the raw $\Delta A(\lambda, t)$ data were corrected for the decay of the initial anisotropy. The correction has the form:

$$\Delta A_{\mathrm{cor}}(\lambda, t) = 2\Delta A(\lambda, t)/[2+r(t)] , \tag{2}$$

where $r(t)$ is the value of the reduced anisotropy measured at 440 nm:

$$r(t) = [\Delta A_{\parallel}(t) - \Delta A_{\perp}(t)]/[\Delta A_{\parallel}(t) + 2\Delta A_{\perp}(t)] . \tag{3}$$

The subscripts $_{\parallel}$ and $_{\perp}$ refer to the polarization of the electric field vector of the probe light with respect to that of the exciting light. Data corrected in this fashion give good agreement with the isotropic average calculated from

$$\Delta A_{\mathrm{av}}(\lambda, t) = \tfrac{1}{3}[\Delta A_{\parallel}(\lambda, t) + 2\Delta A_{\perp}(\lambda, t)] . \tag{4}$$

The ruled grating in the monochromator introduces a slight degree of polarization into the otherwise isotropic probe light. The measured polarization ratio in the 400 to 460 nm region has a maximum value of $I_{\parallel}/I_{\perp} = 1.28$. Consequently, its contribution has been neglected in calculating the correction. The good agreement of the corrected data with the isotropic average confirms that the slight polarization of the probe light can be neglected. All data shown below have been corrected for both photoselection and spectral bandwidth, and for simplicity we shall drop the subscript and refer to the corrected data as $\Delta A(\lambda, t)$.

2.6. Method of analysis

The transient spectra at different times can be viewed as the columns of an $m \times n$ matrix $\Delta A(\lambda, t)$. Several approaches have been described for the global analysis of transient spectral data. The most straightforward approach proceeds by fitting the rows of $\Delta A(\lambda, t)$ to a sum of exponentials. The nonlinear parameters (the rates) are treated globally while the linear parameters (the amplitudes) are treated independently for each wavelength. This approach suffers from the disadvantage that the number of linear parameters scales directly with the number of wavelengths included in the fit.

An alternative approach, which we shall adopt, is based on the supposition that $\Delta A(\lambda, t)$ is likely to be highly singular. The singular value decomposition (SVD) [44,45] of $\Delta A(\lambda, t)$ can be used to determine the size of the null space and to construct a set of orthonormal basis spectra which will span the range of $\Delta A(\lambda, t)$. The application of SVD to the analysis of transient spectra has been described in detail [36,37], and only the salient features are summarized here. According to the theorem of SVD, $\Delta A(\lambda, t)$ can be written as the product of three matrices

$$\Delta A(\lambda, t) = \mathbf{USV}^{\mathrm{T}} \tag{5}$$

$\mathbf{U}$ is an $m \times n$ matrix of orthonormal columns which form a complete set of basis spectra from which the ΔA spectrum at any time can be represented. The column of $\mathbf{U}$ with the largest singular value is the best single-component representation of $\Delta A(\lambda, t)$ in the least-squares sense. The first two columns constitute the best two-component representation, and so on. $\mathbf{S}$ is an $n \times n$ diagonal matrix with nonnegative elements called the singular values. $\mathbf{V}^{\mathrm{T}}$ is the transpose of an $n \times n$ matrix $\mathbf{V}$ having orthonormal rows and columns. Each row of $\mathbf{SV}^{\mathrm{T}}$ contains the set of time-dependent linear coefficients corresponding to each basis spectrum. The tremendous utility of this approach is realized when only a few components are found to be significant. In this case the remainder represent noise and can be considered for all practical purposes to lie in the null space of $\Delta A(\lambda, t)$. In the present application, only a few basis spectra are expected to make significant contributions to $\Delta A(\lambda, t)$. We consider the contribution of a basis spectrum to be significant based on two criteria: the magnitude of its singular value and the autocorrelation of the corresponding column of $\mathbf{V}$.

A third approach to the data analysis is to relate the transient difference spectra to the equilibrium absorption spectra for deoxyMb and MbCO. For small spectral changes, this can be accomplished by representing the transient difference spectra as linear

combinations of the equilibrium spectra and their first and second derivatives. The first derivative contribution is a measure of the band shift, and the second derivative is a measure of the band broadening. If it is assumed that the spectral changes conserve the integrated oscillator strength, then the contributions of the equilibrium spectra are proportional to the survival probability for unligated hemes.

3. Results

3.1. Transient absorption spectra

Transient spectra following photolysis of human MbCO were measured in the Soret region at 250, 270, and 290 K in 75%(w/w) glycerol:buffer, pH 7.0. A small subset of spectra from a 250 K data set are shown in fig. 1A. These spectra were extracted from the original data set at evenly spaced intervals on a logarithmic time scale. The equilibrium absorption spectra of human deoxyMb and MbCO are also shown in fig. 1 along with the difference spectrum deoxyMb(eq)–MbCO(eq). It is clear that the transient spectra at all times resemble the deoxyMb(eq)–MbCO(eq) spectrum.

A closer inspection of the transient spectra in fig. 1A reveals a shift of the positive feature near 436 nm from low to high energy as time progresses. The shift is quantified in fig. 2A where the position of the peak, $\nu(t)$, has been obtained by interpolating from a fit of 15 points of the data in the region of the peak to a fifth-order polynomial. The magnitude of the shift at any time is represented by the quantity

$$\Delta\nu(t) = \nu(t) - \nu(\infty)\,, \qquad (6)$$

where $\nu(\infty)$ is the peak position at a time which is long compared to the time scale of the shift. The magnitude of $\Delta\nu$ at 12 ns ranges from $\approx 50\ \mathrm{cm}^{-1}$ at 250 K to $\approx 20\ \mathrm{cm}^{-1}$ at 290 K. Because the instrument response is 9 ns fwhm, it is expected that these values represent a lower limit for the initial $\Delta\nu$. As seen in fig. 2B, the position of the negative feature near 423 nm does not shift significantly with time. It is therefore likely that the observed shift arises from a change in the deoxyMb spectrum

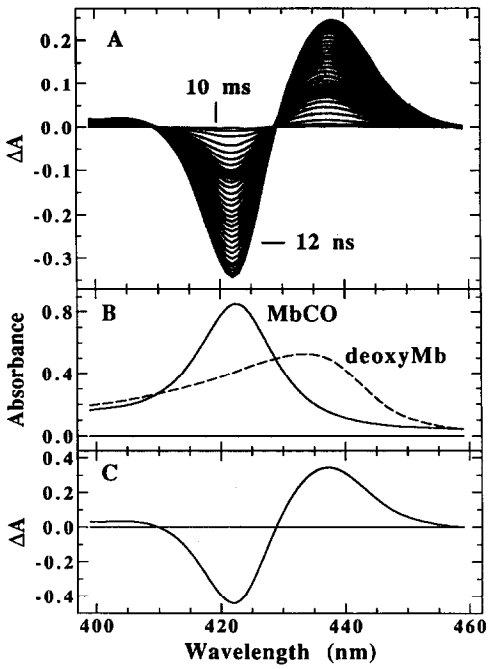

Fig. 1. (A) Transient ΔA spectra at various times following photolysis of MbCO at 532 nm with 8 ns pulses. The transient spectra shown cover the range from 12 ns (largest ΔA) to 10 ms (smallest ΔA) at evenly spaced times on a logarithmic scale. These spectra constitute a small subset of the total data set which consists of 5200 spectra. (B) Absorption spectra of deoxyMb (—) and MbCO(——). (C) The difference spectrum deoxyMb–MbCO. All spectra at 250 K.

3.2. Singular value decomposition

In order to obtain a measure of the ligand rebinding progress curve and to further quantitate the nature and time course of the observed spectral changes, the singular value decomposition of $\Delta A(\lambda, t)$ is utilized as described in the previous section. The basis spectra (columns of **U**) will be referred to as U_1, U_2, ..., the corresponding amplitude vectors (columns of **V**) as V_1, V_2, ..., and the corresponding singular values as S_{11}, S_{22}, ..., respectively. The five largest singular values at each temperature are tabulated in table 1. The remaining singular values are smaller and tend monotonically to zero. SVD of a matrix composed of the points preceding the excitation pulse yields singular values which begin near 0.02 and decrease steadily to zero. This provides a scale for distinguishing signal components from noise compo-

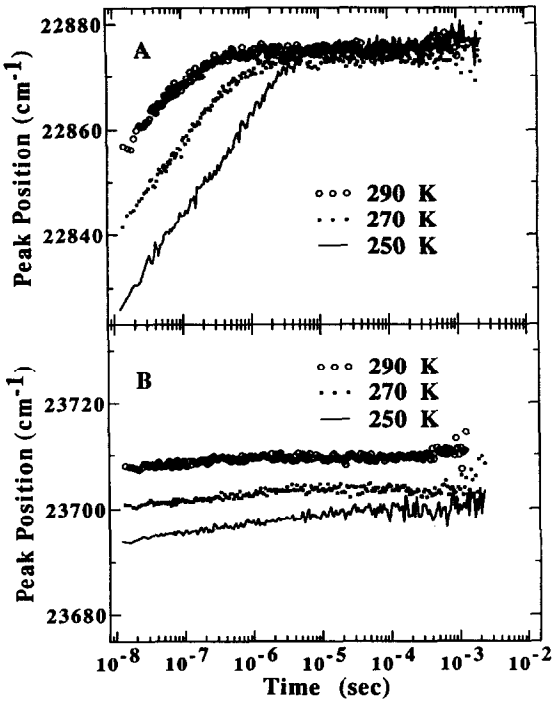

Fig. 2. Time dependence of the low to high energy band shift of the peak near 436 nm in the transient ΔA spectrum following photolysis of MbCO. (A) Position of the peak near 436 nm at 250 K (——), 270 K (■), and 290 K (○). (B) Position of the negative peak near 423 nm at 250 K (——), 270 K (■), and 290 K (●).

Table 1
Singular values

T (K)	S_{11}	S_{22}	S_{33}	S_{44}	S_{55}
250	13.0	0.308	0.0411	0.0275	0.0208
270	13.8	0.234	0.0403	0.0307	0.0249
290	15.1	0.157	0.0288	0.0232	0.0206

nents on the basis of the magnitude of their singular values. Based on this criterion, S_{11} and S_{22} are clearly distinguishable from noise while the rest of the singular values are too small to be distinguished from noise components. A second criterion for distinguishing signal components from noise is based on the autocorrelation of the columns of **V**. As was the case with the singular values, V_1 and V_2 vary smoothly in time, whereas the remaining columns of **V** cannot be distinguished from noise. Consequently, a highly accurate representation of the signal contribution to $\Delta A(\lambda, t)$ can be obtained from a truncated set of basis spectra composed only of U_1 and U_2. The remaining components can be considered to lie in the null space of $\Delta A(\lambda, t)$ to within the signal-to-noise.

The two basis spectra which represent the significant range of $\Delta A(\lambda, t)$ are shown in fig. 3, and their time dependences, contained in the rows of $\mathbf{SV}^T$, are shown in fig. 4. U_1 resembles the deoxyMb(eq)–MbCO(eq) spectrum. Consequently, V_1 is expected to provide a zeroth-order approximation to the ligand rebinding progress curve. Because U_2 crosses zero near 440 nm, V_1 corresponds to the decay of the induced absorption at this wavelength. U_2 has prominent features in the region of the deoxyMb band, but only small features in the region of the MbCO band. This is consistent with the low-to-high energy shift shown in fig. 2. Thus, the most straightforward interpretation of U_2 is that it corresponds to a change in the deoxyMb absorption spectrum. V_2 is therefore

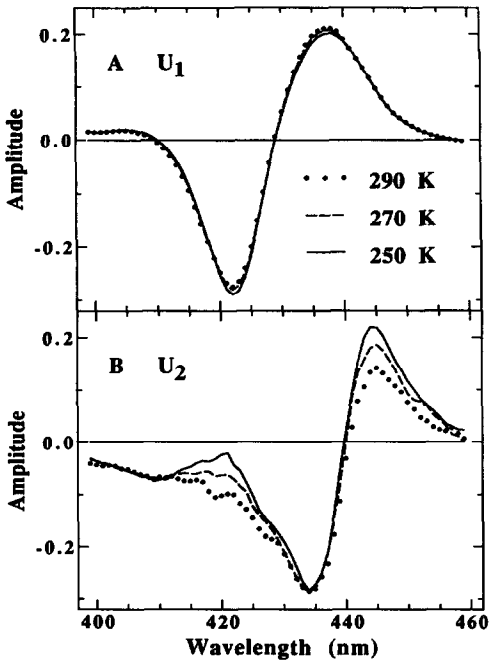

Fig. 3. Singular value decomposition of the data sets at 250 K (——), 270 K (—), and 290 K (●). The two orthonormal basis spectra (columns of **U**) which have the largest singular values are shown (see table 1). (A) The basis spectrum with the largest singular value. (B) The basis spectrum with the second largest singular value.

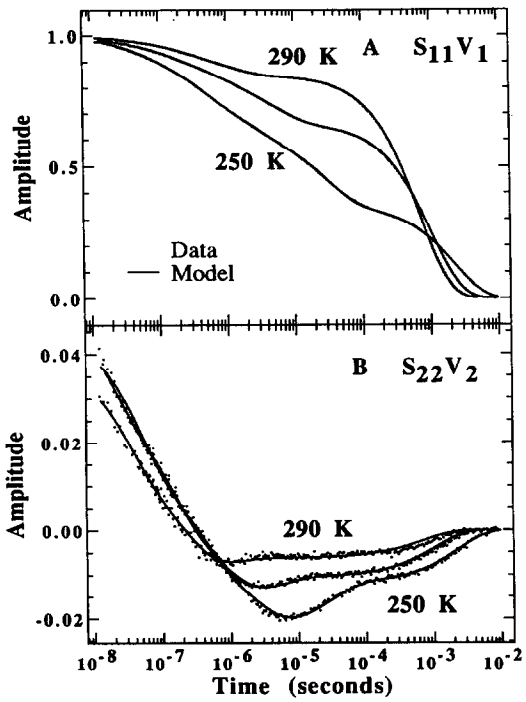

Fig. 4. The time dependent coefficients of the basis spectra (columns of **SV**). Data (···), model (——). (A) Time dependence of the first basis spectrum at 250, 270, and 290 K. (B) Time dependence of the second basis spectrum at 250, 270, and 290 K.

expected to contain the time dependence for the deoxyMb spectral change. Note that even if the relative contributions of U_1 and U_2 do not change, the amplitude of V_2 still diminishes with time as the overall signal decays due to ligand rebinding. Therefore, V_2 contains information regarding not only the deoxyMb spectral evolution, but also rebinding to both unrelaxed as well as relaxed species.

A more concise representation of the time courses for the basis spectra can be obtained by simultaneously fitting the columns of **V** to a sum of exponentials

$$C_i(t) = \sum_j a_{ij} \exp[-t/\tau_j] , \qquad (7)$$

where $C_i(t)$ is the model function for the ith column of **V**. The time constants τ_j are varied globally over the columns of **V** while the amplitudes, a_{ij}, are found independently for each column. The number of time constants was chosen to give a good fit to V_1, and the same set of time constants also provides a good fit to V_2. The parameters from the simultaneous fits are listed in table 2 and the model traces are overlaid with the data in fig. 4.

The observation of two significant basis spectra implies the existence of a minimum of two spectral components, $D_1(\lambda)$ and $D_2(\lambda)$, which will subsequently be referred to as unrelaxed and relaxed deoxyMb, respectively. If the spectra for both components were known beforehand, it would be possible to calculate the time course for the corresponding populations directly from the experimental data by finding the linear combination of these two spectra $\Delta A_m(\lambda, t)$ which best fits the transient spectra at each time

$$\Delta A_m(\lambda, t) = b_1(t) D_1(\lambda) + b_2(t) D_2(\lambda) . \qquad (8)$$

The spectrum for relaxed deoxyMb $D_2(\lambda)$ corresponds to the spectrum observed during the bimolecular recombination process. This spectrum is readily calculated as a linear combination of the basis spectra with coefficients determined from the bimolecular amplitudes in table 2. This spectrum is then normalized to unit population assuming that V_1 is proportional to the fraction of unliganded Mbs. The spectrum of unrelaxed deoxyMb $D_1(\lambda)$, on the other hand, is not specified uniquely from the data alone. Assuming unit population for the unrelaxed deoxyMb at zero time, two cases will be considered. In the first case, it is assumed that all of the relaxation occurs within the time window of observation. The spectrum of unrelaxed deoxyMb is then calculated using eq. (7) as

$$D_1(\lambda) = C_1(0) U_1 + C_2(0) U_2 . \qquad (9)$$

These spectra and their corresponding population time courses are shown in figs. 5 and 6. In the second case we consider the possibility that some of the relaxation occurs during the laser pulse and is therefore not observed. Assuming that the initial shift of the unrelaxed deoxyMb band does not depend on temperature, the unrelaxed deoxyMb spectrum is estimated from the data in fig. 2 using

$$\Delta A(\lambda, 12\ ns) = \alpha D_1(\lambda) + (1-\alpha) D_2(\lambda) , \qquad (10)$$

where $\alpha = \Delta\nu(12\ \text{ns})/\Delta\nu(0)$. Because the value of $\Delta\nu(0)$ is not determined in this experiment, we use a value of 140 cm^{-1} reported for the shift of deoxyMb* at cryogenic temperatures [46]. This value

Table 2
Summary of model parameters

T (K)	Parameter [a]	Exponential component (j)				
		1	2	3	4	5
250	a_{1j}	0.06	0.17	0.15	0.27	0.35
	a_{2j}	0.032	0.020	0.017	−0.011	−0.012
	a_{uj}	0.40	0.30	0.25	−0.02	0
	a_{rj}	−0.33	−0.13	−0.11	0.29	0.35
	τ_j	46 ns	370 ns	2.4 μs	31 μs	2.2 ms
270	a_{1j}	0.01	0.07	0.09	0.17	0.66
	a_{2j}	0.024	0.027	0.018	−0.005	−0.010
	a_{uj}	0.36	0.40	0.28	−0.03	0
	a_{rj}	−0.34	−0.34	−0.18	0.20	0.66
	τ_j	17 ns	134 ns	840 ns	5.8 μs	1.1 ms
290	a_{1j}	–	0.01	0.05	0.09	0.85
	a_{2j}	–	0.025	0.023	−0.002	−0.006
	a_{uj}	–	0.54	0.50	−0.04	0
	a_{rj}	–	−0.53	−0.44	0.12	0.85
	τ_j	–	31 ns	210 ns	1.2 μs	710 μs

[a] a_{1j} and a_{2j} are the amplitudes and τ_j is the time constant from the simultaneous fit of eq. (7) to the columns of **SV** in fig. 4. The amplitudes a_{uj} and a_{rj} were calculated for the unrelaxed and relaxed populations in fig. 6 using the time constants from the simultaneous fit to **SV**.

is likely to represent an upper limit on $\Delta\nu(0)$. The spectra and corresponding population time courses for this case are shown in figs. 7 and 8.

The normalized time course of the first SVD component provides an approximation to the ligand rebinding progress curve. Evidently the accuracy of this approximation increases as the relative contributions from the other basis spectra decrease. The uncertainty depends not only on the magnitude of the spectral changes but explicitly on their shape as well. The ability of V_1 to approximate the time course for ligand rebinding is determined by how similar the least-squares spectral change (V_2) is to the actual spectral change. After some time, the transient spectra have attained the shape of the final intermediate, and V_1 then faithfully monitors ligand rebinding. The greatest uncertainty in V_1 occurs at early time. In order to estimate the magnitude of the uncertainty in V_1, $\Delta A(\lambda, t)$ was fit to a linear combination of $A_{\mathrm{MbCO}}(\lambda, t)$, $A_{\mathrm{Mb}}(\lambda, t)$, and first and second derivatives of $A_{\mathrm{Mb}}(\lambda, t)$. In test cases, the coefficients of $A_{\mathrm{MbCO}}(\lambda, t)$ were generally a good monitor of ligand rebinding. As expected, the approximate ligand rebinding curves obtained by these two methods agree quantitatively on the long-time scale. The overall agreement is best at 290 K and worst at 250 K. At 250 K, the maximum discrepancy occurs at early time where it appears that the two estimates differ by 3%.

4. Discussion

The results of the preceding analysis are consistent with the division of the recombination reaction into three kinetic stages. This is most clearly evident in the data at 250 K. During the first stage, ligand recombination is accompanied by a change in the deoxyMb absorption spectrum. The kinetics of the ligand recombination as well as the spectral change are both multi-exponential. No significant spectral changes are observed during the subsequent kinetic stages and the transient spectra are indistinguishable from the equilibrium deoxyMb–MbCO spectrum. Single exponential kinetics are observed during the intermediate stage. The final kinetic stage is distinguished from the others both temporally and by its dependence on the concentration of CO (data not shown). This stage can be immediately identified with the process of bimolecular recombination of CO from bulk solution. Under the conditions of our experi-

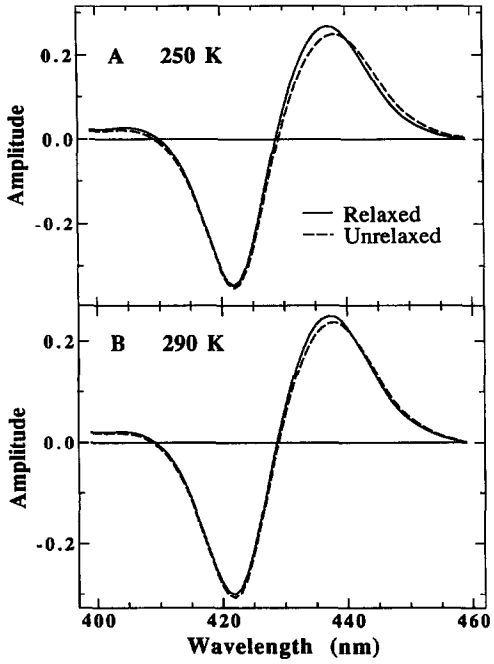

Fig. 5. ΔA spectra of unrelaxed (—) and relaxed (——) deoxyMb at (A) 250 K, and (B) 290 K. The spectrum of the unrelaxed intermediate was calculated from the simultaneous fit to V_1 and V_2 assuming that the entire relaxation has been observed.

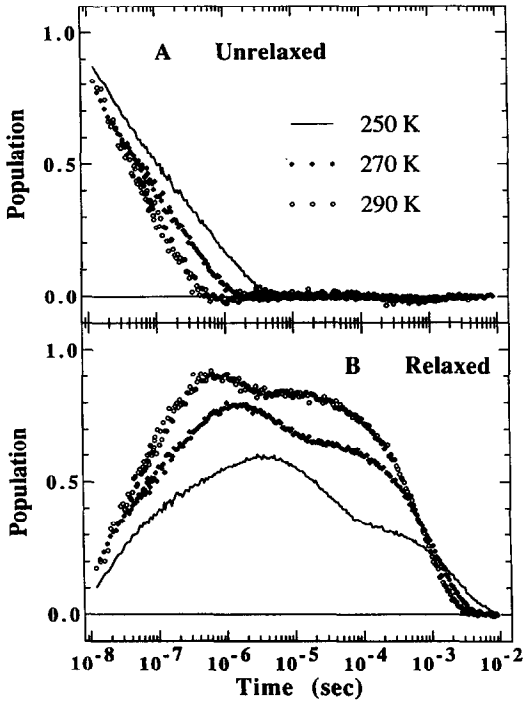

Fig. 6. Time dependence of the deoxyMb intermediates (see fig. 5) at 250 K (——), 270 K (♦), and 290 K (○). (A) Time dependence of the unrelaxed deoxyMb intermediate. (B) Time dependence of relaxed deoxyMb.

ments ([CO] ≫ [Mb] at all times), the kinetics are pseudo-first order and consequently a single exponential decay is observed. These results are qualitatively similar to the data for sperm whale Mb obtained under similar experimental conditions [10,15].

Several experiments have demonstrated the existence of metastable intermediates following the photolysis of MbCO at cryogenic temperatures [14–16,19,27,46]. At low temperatures, spectral changes in band III of the MbCO photoproduct have been shown to result from a kinetic hole burning mechanism [17]. Near the glass transition of 75% glycerol:water (180–220 K), relaxation also contributes to the spectral changes [15,46]. Steinbach et al. [15] have used a stretched exponential model for the relaxation of Mb* which agrees well with their data for sperm whale Mb, particularly in the region of the glass transition. The relaxation function has the form

$$\Phi(t, T) = \exp\{-[\kappa(T)t]^{\beta}\}, \qquad (11)$$

where

$$\kappa(T) = A \exp[-(E/RT)^2] .$$

Using their values of $A = 10^{18}\ s^{-1}$, $E = 10$ kJ/mol and $\beta = 0.24$, the relaxation predicted by eq. (11) is overlaid with the population time courses in fig. 8. At 250 K, the relaxation predicted by eq. (11) appears to agree reasonably well with the time course for the decay of unrelaxed deoxyMb. At higher temperatures, however, the model deviates significantly from the observed relaxation. This is not entirely unexpected since $\kappa(T)$ tends to a physically unreasonable rate of $10^{18}\ s^{-1}$ in the high-temperature limit. Because ligand rebinding to the unrelaxed deoxyMb also contributes to the population time course, the actual discrepancy may be larger. If $\Delta\nu(0)$ is less than 140 cm^{-1} then the discrepancy will be larger at all three temperatures (c.f. fig. 6A). If $\Delta\nu(0)$ is greater than 140 cm^{-1} then the agreement becomes worse at 250 K while improving somewhat at the higher temperatures.

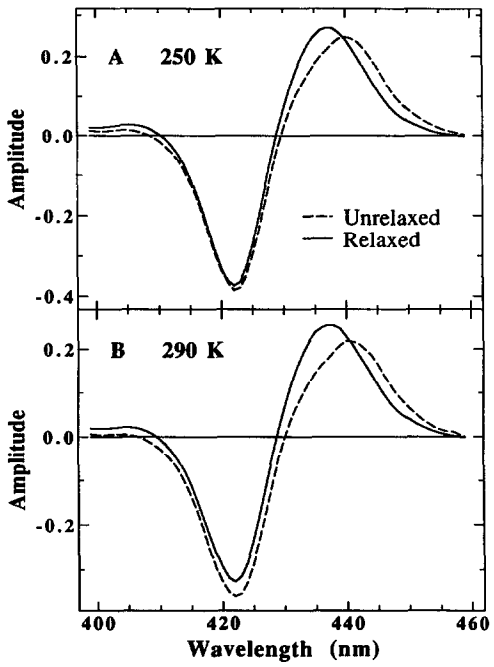

Fig. 7. ΔA spectra of unrelaxed (—) and relaxed (——) deoxyMb at (A) 250 K and (B) 290 K. The spectrum of the unrelaxed intermediate was calculated based on the assumption that some portion of the relaxation occurs on a timescale to fast to be observed in this experiment. See text for details.

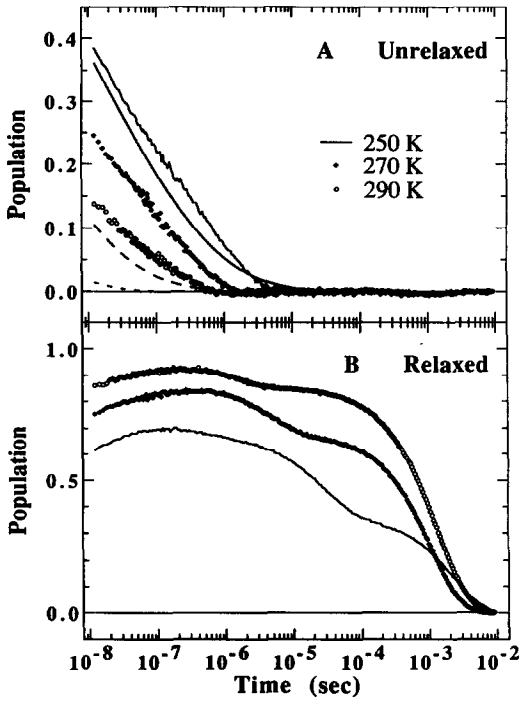

Fig. 8. Time dependence of the deoxyMb intermediates (see fig. 7) at 250 K (——), 270 K (♦), and 290 K (○). (A) Time dependence of the unrelaxed deoxyMb intermediate. Overlaid with the data are the model curves for the stretched exponential relaxation function from Steinbach et al. [15]. (B) Time dependence of relaxed deoxyMb.

Another important observation is that only two significant components are obtained from the SVD, even though the kinetics for the spectral evolution are multi-exponential. This sort of behavior is also seen in the spectral changes which accompany structural relaxation in Hb [38]. In fact, strong qualitative similarities exist between the spectral changes in Mb and the spectral changes which have been reported in the Soret region of Hb [36] and iron–cobalt hybrid Hbs [37]. The most significant similarity is in the overall shape of the spectral change. In both cases, the second basis spectrum, U_2, exhibits a strong feature near the peak of the deoxy band, and a feature of the opposite sign which occurs to the red of this while little change is observed near the peak of the absorption for the CO form. This lends further support to the suggestion that structural relaxations of the protein are coupled to the heme electronic transitions via a common coordinate [38,46]. One reasonable proposal is that the deoxyMb spectral changes result from changes in the out-of-plane displacement of the heme iron along the iron–proximal histidine bond coordinate [35,38,46].

4.1. Origin of the deoxy Mb spectral changes

The physical origin of the spectral changes will ultimately determine their functional significance. There are at least two distinct mechanisms which have been shown to contribute to spectral evolution in Mb: kinetic hole burning and structural relaxation. Although rebinding to unrelaxed intermediates of deoxyMb (kinetic hole burning) probably contributes to the observed spectral evolution [17], it is likely that a significant (if not the predominant) contribution in the temperature range above 220 K arises from a structural relaxation of the protein. The driving force for these relaxations is provided by the difference in free energy between deoxyMb at equi-

librium and deoxyMb distorted along the coordinates which take it into the structure of MbCO. This difference in free energy is a function not only of the tertiary structure of the protein but also involves reorganization of the solvent in response to the structural changes. The relaxations might be coupled to solvent dynamics either through exchange dynamics amongst solvent molecules associated with the protein [47–49] or through the damping of protein motions under the influence of solvent viscosity [50,51].

4.2. Coupling of structural relaxation and kinetics

An important and as yet unresolved question concerns the coupling between the structural relaxation and the kinetics. One possibility is that the structural relaxation alters the barriers for rebinding [15,34] and is thus partly responsible for the multi-exponential kinetics that are observed for the rebinding process. In this case, the barriers for rebinding during the first kinetic stage are not involved in determining the rates of recombination to the thermally averaged protein. An alternative is that spectral changes are the passive response to ligand migration in the protein [36–38], perhaps as the result of exchange of the ligand and solvent molecules between the protein interior and solvent, or collapse of the hydrophobic protein interior into the void that is left behind as the ligand escapes into the solvent. In this case the relaxation is not expected to affect the rates of recombination or escape, but rather the rate of escape is expected to determine the rate for structural relaxation.

In conclusion, the spectral changes in Soret band of deoxyMb are indicative of protein structural relaxations which are coupled to and therefore detectable via electronic transitions. The fact that a significant amount of ligand rebinding occurs on the same timescale as the spectral evolution suggests that kinetic hole burning may also contribute. As is the case in Hb, the character of the deoxyMb spectral changes is complex and cannot be interpreted as a simple band shift. The similarity between the spectral changes in Hb and Mb (corresponding to different structural changes) provides additional evidence that the Soret spectral changes are indirectly coupled to the structural relaxations by a common coordinate [38]. The nonexponential kinetics and spectral changes observed during the first kinetic stage can be interpreted in terms of an underlying inhomogeneous distribution of solvent/protein environments which is unrelaxed on a timescale less than about τ_3. On a timescale which is longer than τ_3, the distribution is effectively averaged insofar as ligand rebinding and the Soret spectral changes are concerned as suggested for sperm whale Mb [15].

Acknowledgement

We are grateful to Drs. Jim Hofritcher, Bill Eaton, and Anjum Ansari for helpful discussion regarding the application of SVD to the analysis of transient spectra. This work is supported by the NIH grant (GM27738).

References

[1] J.C. Kendrew, R.E. Dickerson, B.E. Strandberg, R.G. Hart, D.R. Davies, D.C. Phillips and V.C. Shore, Nature (London) 185 (1960) 422.
[2] M.F. Perutz and F.S. Matthews, J. Mol. Biol. 21 (1966) 199.
[3] C.L. Nobbs, in: Hemes and Heme Proteins, eds. B. Chance, R.W. Eastbrook, and T. Yonetani (Academic Press, New York, 1966) p. 143.
[4] T. Takano, J. Mol. Biol. 110 (1977) 537.
[5] T. Takano, J. Mol. Biol. 110 (1977) 596.
[6] M.F. Perutz, Nature (London) 228 (1970) 726.
[7] J.M. Baldwin and C. Chothia, J. Mol. Biol. 129 (1979) 175.
[8] D.A. Case and M. Karplus, J. Mol. Biol. 132 (1979) 344.
[9] Q.H. Gibson, J. Physiol. (London) 136 (1956) 112.
[10] R.H. Austin, K.W. Beeson, L. Eisenstein, H. Frauenfelder and I.C. Gansalus, Biochemistry 14 (1975) 5355.
[11] B.B. Hasinoff, Arch. Biochem. Biophys. 183 (1977) 176.
[12] D. Beece, L. Eisenstein, H. Frauenfelder, D. Good, M.C. Marden, L. Reinisch, A.H. Reynolds, L.B. Sorensen and K.T. Yue, Biochemistry 19 (1980) 5147.
[13] W. Doster, D. Beece, S.F. Bowne, E.E. DiIorio, L. Eisenstein, H. Frauenfelder, L. Reinisch, E. Shyamsunder, K.H. Winterhalter and K.T. Yue, Biochemistry 21 (1982) 4831.
[14] T. Iizuka, H. Yamamoto, M. Kotani and T. Yonetani, Biochim. Biophys. Acta 371 (1974) 1715.
[15] P.J. Steinbach, A. Ansari, J. Berendzen, D. Braunstein, K. Chu, B.R. Cowen, D. Ehrenstein, H. Frauenfelder, J.B. Johnson, D.C. Lamb, S. Luck, J.R. Mourant, G.U. Nienhaus, P. Ormos, R. Philip, A. Xie and R.D. Young, Biochemistry 30 (1991) 3988.
[16] A. Ansari, J. Berendzen, S.F. Bowne, H. Frauenfelder, I.E.T. Iben, T.B. Sauke, E. Shyamsunder and R.D. Young, Proc. Natl. Acad. Sci. USA 82 (1985) 5000.

[17] B.F. Campbell, M.R. Chance and J.M. Friedman, Science 238 (1987) 373.
[18] N. Agmon, Biochemistry 27 (1988) 3507.
[19] P. Ormos, A. Ansari, D. Braunstein, B.R. Cowen, H. Frauenfelder, M.K. Hong, I.E.T. Iben, T.B. Sauke, P. Steinbach and R.D. Young, Biophys. J. 57 (1990) 191.
[20] I.E.T. Iben, D. Braunstein, W. Doster, H. Frauenfelder, M.K. Hong, J.B. Johnson, S. Luck, P. Ormos, A. Schulte, P.J. Steinbach, A.H. Xie and R.D. Young, Phys. Rev. Letters 62 (1989) 1916.
[21] H. Frauenfelder, N.A. Alberding, A. Ansari, D. Braunstein, B.R. Cowen, M.K. Hong, I.E.T. Iben, J.B. Johnson, S. Luck, M.C. Marden, J.R. Mourant, P. Ormos, L. Reinisch, R. Scholl, A. Schulte, E. Shyamsunder, L.B. Sorensen, P. Steinbach, A. Xie, R.D. Young and K.T. Lee, J. Phys. Chem. 94 (1990) 1024.
[22] J.-L. Martin, A. Migus, C. Poyart, Y. Lecarpentier, R. Astier and A. Antonetti, Proc. Natl. Acad. Sci. USA 80 (1983) 173.
[23] R. Lingle, X. Xu, H. Zhu, S. Yu and J.B. Hopkins, J. Am. Chem. Soc. (1991), submitted.
[24] S.M. Janes, G.A. Dalickas, W.A. Eaton and R.M. Hochstrasser, Biophys. J. 54 (1988) 545.
[25] E.R. Henry, J.H. Sommer, J. Hofrichter and W.A. Eaton, J. Mol. Biol. 166 (1983) 443.
[26] E.W. Findsen, T.W. Scott, M.R. Chance, J.M. Friedman and M.R. Ondrias, J. Am. Chem. Soc. 107 (1985) 3355.
[27] D.L. Rousseau and P.V. Argade, Proc. Natl. Acad. Sci. USA 83 (1986) 1310.
[28] J.M. Friedman, R.A. Stepnoski, M. Stavola and M.R. Ondrias, Biochemistry 21 (1982) 2022.
[29] S. Dasgupta, T.G. Spiro, C.K. Johnson, G.A. Dalickas and R.M. Hochstrasser, Biochemistry 24 (1985) 5295.
[30] J.A. Westrick, J.L. Goodman and K.S. Peters, Biochemistry 26 (1987) 8313.
[31] L. Genberg, L. Richard, G. McLendon and R.J.D. Miller, Science 251 (1991) 1051.
[32] X. Xie and J.D. Simon, Biochemistry 30 (1991) 3682.
[33] J.W. Petrich, J.C. Lambry, K. Kuczera, M. Karplus, C. Poyart and J.-L. Martin, Biochemistry 30 (1991) 3975.
[34] N. Agmon and J.J. Hopfield, J. Chem. Phys. 79 (1983) 2042.
[35] V. Srajer, L. Reinisch and P.M. Champion, J. Am. Chem. Soc. 110 (1988) 6656.
[36] J. Hofrichter, J.H. Sommer, E.R. Henry and W.A. Eaton, Proc. Natl. Acad. Sci. USA 80 (1983) 2235.
[37] J. Hofrichter, E.R. Henry, J.H. Sommer, R. Deutsch, M. Ikeda-Saito, T. Yonetani and W.A. Eaton, Biochemistry 24 (1985) 2667.
[38] L.P. Murray, J. Hofrichter, E.R. Henry, M. Ikeda-Saito, K. Kitagishi, T. Yonetani and W.A. Eaton, Proc. Natl. Acad. Sci. USA 85 (1988) 2151.
[39] S. Balasubramanian, D.G. Lambrigt, M.C. Marden and S.G. Boxer, manuscript in preparation.
[40] R. Varadarajan, A. Szabo and S.G. Boxer, Proc. Natl. Acad. Sci. USA 82 (1985) 5681.
[41] R. Varadarajan, D.G. Lambright and S.G. Boxer, Biochemistry 28 (1989) 3771.
[42] A. Ansari, C. Jones, E.R. Henry, J. Hofrichter, W.A. Eaton and A. Szabo, Fogarty Intern. Conf. on The Dynamics and Kinetics of Myoglobin and Hemoglobin.
[43] A. Ansari, C. Jones, E.R. Henry, J. Hofrichter, W.A. Eaton and A. Szabo, Biophys. J. 59 (1991) 286a.
[44] G.H. Golub and C. Reinsch, Numer. Math. 14 (1970) 403.
[45] R.I. Shrager and R.W. Hendler, Anal. Chem. 54 (1982) 1147.
[46] V. Srajer and P.M. Champion, Biochemistry 30 (1991) 7390.
[47] S.V.E. Phillips, J. Mol. Biol. 142 (1980) 531.
[48] H.D. Middendorf and J. Randall, Phil. Trans. Roy. Soc. London Ser. B 290 (1980) 639.
[49] R.F. Goldstein and W. Bialek, Comments Mol. Cell. Biophys. 3 (1986) 407.
[50] B. Somogyi and S. Damjanovich, J. Theoret. Biol. 48 (1975) 393.
[51] B. Gavish, Biophys. Struct. Mech. 4 (1978) 37.